energies

MDPI

Communication

Multiscale Molecular Dynamics Simulations of Fuel Cell Nanocatalyst Plasma Sputtering Growth and Deposition

Pascal Brault

GREMI CNRS-Université d'Orléans BP6744, 14 rue d'Issoudun, CEDEX 2, 45067 Orléans, France; pascal.brault@univ-orleans.fr

Received: 17 June 2020; Accepted: 9 July 2020; Published: 11 July 2020

Abstract: Molecular dynamics simulations (MDs) are carried out for predicting platinum Proton Exchange Membrane (PEM) fuel cell nanocatalyst growth on a model carbon electrode. The aim is to provide a one-shot simulation of the entire multistep process of deposition in the context of plasma sputtering, from sputtering of the target catalyst/transport to the electrode substrate/deposition on the porous electrode. The plasma processing reactor is reduced to nanoscale dimensions for tractable MDs using scale reduction of the plasma phase and requesting identical collision numbers in experiments and the simulation box. The present simulations reproduce the role of plasma pressure for the plasma phase growth of nanocatalysts (here, platinum).

Keywords: plasma sputtering; molecular dynamics; multiscale modeling; nanocatalyst; PEM fuel cell electrodes; gas aggregation source

1. Introduction

Efficient design of nanocatalysts for use in proton exchange membrane fuel cells has attracted a lot of interest [1,2]. Since platinum nanoparticles (NPs) are known as the best catalyst, efforts have focused on reducing its content either by optimizing size, dispersing in the electrode, or alloying with more common or less critical metal atoms [3]. To this end, many synthesis techniques such as plasma sputtering deposition have been investigated, including conventional magnetron, high-power impulse magnetron sputtering, and magnetron gas aggregation source depositions [4–7]. Since these deposition processes are of atomic nature, the description and insights into targeted growth processes to improve NP morphology, structure, and properties can successfully be explored using atomistic simulations, especially molecular dynamics [8–16]. Both growth in inert and reactive plasma environments has, thus, been shown feasible. While focusing on the deposition process, the initial conditions of the simulations should be extracted from experiments to reach a suitable quality of comparison and/or prediction. This includes temperatures, velocity distribution of the sputtered species, and composition of the plasma phase. A better way would be to simulate the whole sputtering/deposition/growth process occurring in these techniques. A preliminary attempt has been realized considering atomic deposition, at low pressure (2.5 Pa) from conventional sputtering [13]. The simulation box included a platinum target, the plasma forming gas (argon here), and the substrate (a model porous Vulcan carbon [17] for mimicking a fuel cell uncatalyzed electrode). The simulation box dimensions, and then the atom numbers required for the simulation, are dictated by the dissipation of energy during impact on the target and substrate. The argon vapor, between the target and substrate, is intended to mimic the plasma forming gas. The density of this vapor in the simulation box is determined by assuming that the collision number along the target to substrate path is the same as in experiments, which leads to equal (pressure) × (target-to-substrate distance) products in experiments (P_{exp}, d_{exp}) and in the

simulation box (P_{sim}, d_{sim}): $P_{exp} \cdot d_{exp} = P_{sim} \cdot d_{sim}$. Sputtering ions are randomly created above the target to impact the target platinum atoms at the desired kinetic energy, i.e., corresponding to the target bias voltage. Sputtering, thus, freely occurs without any constraint. A specific study of the sputtering of a platinum target using MDs has been conducted to determine the kinetic energy distributions of sputtered platinum for different argon ions impinging energies [11]. Such a model will be able to describe conventional magnetron sputtering at low pressure while it will be relevant for magnetron sputtering powered gas aggregation sources cluster growth.

The present work will focus on the multiscale simulation of the sputtering and deposition process at higher pressure, 7.5 Pa, for which nucleation of Pt NPs in the plasma phase is expected to occur. The resulting deposited NPs on the model carbon fuel cell electrode are compared to the low-pressure case (2.5 Pa) for which no NPs are produced in the plasma phase, i.e., during travelling from the target to the fuel cell electrode.

2. Materials and Methods

The simulation box was built considering a large enough width of 12 × 12 nm^2, allowing NP growth up to 4 nm in diameter. The Pt target height was 10 nm (96,100 Pt atoms), while the carbon substrate thickness was 6 nm (68,160 C atoms). The height of the space between the target and the electrode was chosen to mimic an experimental argon pressure of 7.5 Pa for an experimental target to substrate separation of 6.5 cm. Applying the equality of collision numbers in the simulation box and the experiment [13,18] led to a height of 120 nm and 17,388 Argon atoms. The corresponding simulation box is drawn in Figure 1.

Molecular dynamics simulations (MDs) solve the Newton equations of motion (or Langevin dynamics, which includes energy dissipation through an additional friction term) as follows:

$$\frac{\partial^2}{\partial t^2}\vec{r_i} = \frac{1}{m_i}\vec{f}_i, \vec{f}_i = -\vec{\nabla}V(\vec{r}_1(t), \vec{r}_1(t), \cdots, \vec{r}_1(t)) \quad (1)$$

where $\vec{r}_i(t)$ is the position of atom i at time t with mass m_i, and V is the interaction potential between all involved species. So, solving such a set of equations requires knowledge of the interaction potential V and a set of initial conditions, say positions and velocities, preferably matching experimental situations.

While carbon and platinum atoms are located at their solid-state position, the space between the Pt target and C substrate is filled by the randomly located Ar atoms. The initial velocities of all atoms were randomly selected in a Maxwell–Boltzmann distribution at 300 K. For mimicking ion creation in the zone above the target as it occurs during magnetron sputtering, 500 argon atoms were randomly chosen to be converted to ions with a kinetic energy directed towards the Pt target. The chosen kinetic energy was 500 eV, as typical in related experiments [18]. The timestep for solving the equation was 0.1 fs. Such a short timestep is required for proper sampling of the Ar-Pt interaction potential at such high kinetic energies. The Pt-Pt interactions are described by the Embedded Atom Method (EAM) [11,19], C-C by the Tersoff potential [20], and repulsive Ar-Pt and Ar-C by the Moliere form [21]. Pt-C interactions are modeled by an improved Lennard–Jones potential [9,22]. Damping time for Berendsen thermostats used for dissipating energy in the plasma region through Ar gas, in the carbon substrate and in the platinum target was 1 ps. The calculations lasted for 2 ns: 500 Ar ions were successively created and released to the Pt every 2 ps. Additional 1 or 2 ns time was needed and added for allowing created Pt atoms to travel and interact with the carbon substrate. Simulations were built and run using LAMMPS software [23,24].

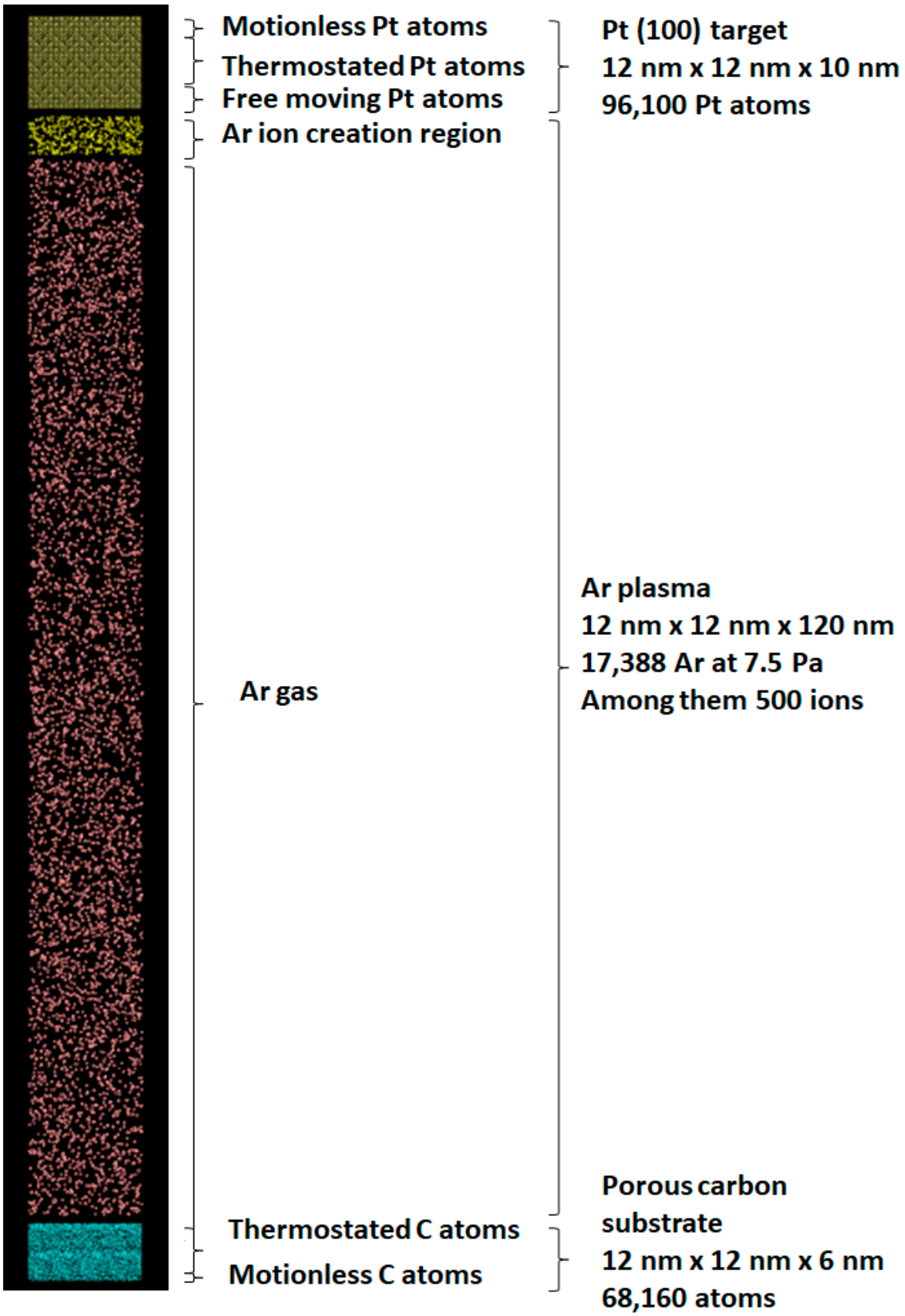

Figure 1. Schematics of the simulation cell with the initial positions of all species involved in the sputtering plasma simulation.

3. Results and Discussion

Figure 2 displays side views of the deposition process for two Ar pressures: 2.5 Pa, 2 ns and 7.5 Pa, 3 ns. As can be seen, despite 1 or 2 ns additional time elapsing after last ion was released from the target, some Pt atoms (2.5 Pa) and Pt nanoclusters (7.5 Pa) always traveled from the target to the substrate. At 7.5 Pa, since there were more collisions, the mean kinetic energy of Pt atoms and nanoclusters was lowered compared to 2.5 Pa; thus, Pt species were longer retained in the gas phase.

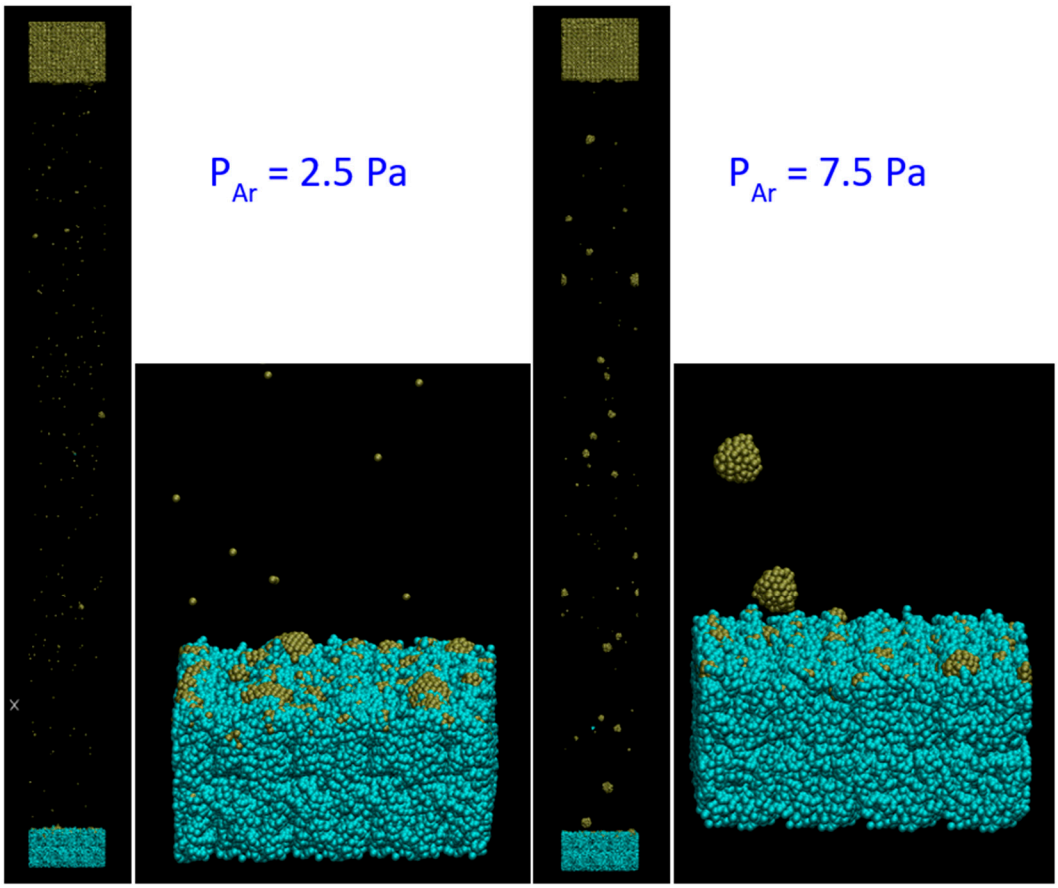

Figure 2. Snapshots of the whole deposition frames and magnification on the carbon electrode at P = 2.5 Pa, t = 2 ns and P = 7.5 Pa, t = 3 ns. Argon atoms have been removed for clarity.

Snapshots of the Pt nanocluster grown from atomic motion at P = 2.5 Pa and grown from a mixing of atoms and nanoclusters are shown in Figure 3. Both were recorded at 2 ns.

When comparing depositions at the same time, t = 2 ns, the deposited Pt amount was 6.4×10^{14} atoms·cm^{-2} at P = 7.5 Pa while it was 17.3×10^{14} atoms·cm^{-2} at P = 2.5 Pa. The sputtering yields were close together, i.e., 5.4 at 7.5 Pa and 6.4 at 2.5 Pa. So, the difference between the two Pt coverages clearly originated from the different Ar pressures and, thus, the different travel times. When increasing the deposition time (without additional sputtering) at 7.5 Pa, the deposited Pt amount increased to 8.3×10^{14} atoms·cm^{-2}. While Pt travel time increased for P = 7.5 Pa, Pt atoms had time to collide among themselves to form NPs during transport to the substrate. Thus, part of the deposit at this pressure originated from gas phase NPs and smaller NPs formed by Pt-Pt interactions on the porous carbon surface, as for P = 2.5 Pa. Looking at 3 ns time, Figure 2 shows that the largest clusters were deposited later. This comes from the growing and travel time needed for reaching a larger size in the gas phase. Additionally, the velocity of large NPs is lower than that for smaller ones. This is

consistent with mass spectrometry measurements [6,25]. The width of the box is dependent of the maximum reachable NP size; in the present case it was 2 nm, that is to say 17% of the box width.

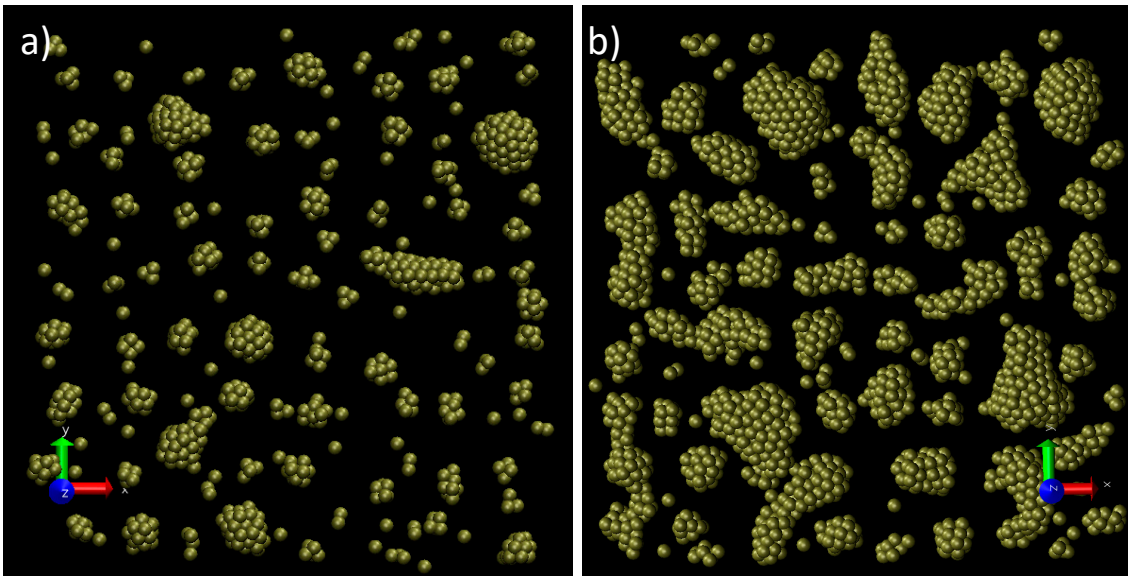

Figure 3. Snapshots of the Pt deposits at 2 ns (**a**) 7.5 Pa and (**b**) 2.5 Pa. Carbon atoms have been removed for clarity.

Since more Pt atoms have been deposited at low pressure, the nanocluster size is higher. Nanoclusters are crystalline in both situations. It should be noticed that NPs grown in the gas phase were already crystalline too, in agreement with experimental findings of gas aggregation source NP growth [6,25].

4. Conclusions

Molecular dynamics simulations are shown to be able to describe and predict NP growth, both in conventional sputtering and in sputtering powered gas aggregation source in modeling the whole multiscale process in a one-shot simulation. This is made possible by a scaling down of the space between the target and substrate based on conserving the collision number in experiments and the simulation box. The focus on the high-pressure regime, relevant for gas-aggregation source modeling, shows a lower deposition rate and fewer crystalline NPs on the substrate, in agreement with experimental findings.

Funding: This research received no external funding.

Acknowledgments: Amaël Caillard is gratefully acknowledged for highlighting discussions.

Conflicts of Interest: The author declares no conflict of interest.

References

1. Antolini, E. Recent Developments in Polymer Electrolyte Fuel Cell Electrodes. *J. Appl. Electrochem.* **2004**, *34*, 563–576. [CrossRef]
2. Litster, S.; McLean, G. PEM fuel cell electrodes. *J. Power Sources* **2004**, *130*, 61. [CrossRef]
3. Greeley, J.; Stephens, I.E.L.; Bondarenko, A.S.; Johansson, T.P.; Hansen, H.A.; Jaramillo, T.F.; Rossmeisl, J.; Chorkendorff, I.; Nørskov, J.K. Alloys of platinum and early transition metals as oxygenreduction electrocatalysts. *Nat. Chem.* **2009**, *1*, 552–556. [CrossRef] [PubMed]
4. Brault, P.; Caillard, A.; Thomann, A.L. Polymer electrolyte fuel cell electrodes grown by vapor deposition techniques. *Chem. Vap. Depos.* **2011**, *17*, 296–304. [CrossRef]

5. Cuynet, S.; Caillard, A.; Lecas, T.; Bigarre, J.; Buvat, P.; Brault, P. High Power Impulse Magnetron Sputtering deposition of Pt inside fuel cell electrodes. *J. Phys. D Appl. Phys.* **2014**, *47*, 272001. [CrossRef]
6. Caillard, A.; Cuynet, S.; Lecas, T.; Andreazza, P.; Mikikian, M.; Thomann, A.L.; Brault, P. PdPt catalyst synthesized by gas aggregation source and magnetron sputtering for fuel cell electrodes. *J. Phys. D Appl. Phys.* **2015**, *48*, 475302. [CrossRef]
7. Brault, P. Review of low pressure plasma processing of proton exchange membrane fuel cell electrocatalysts. *Plasma Process. Polym.* **2016**, *13*, 10–18. [CrossRef]
8. Bauchire, J.-M.; Thomann, A.-L.; Bedra, L. Molecular Dynamics simulations of clusters and thin film growth in the context of plasma sputtering deposition. *J. Phys. D Appl. Phys.* **2014**, *47*, 224004.
9. Xie, L.; Brault, P.; Coutanceau, C.; Caillard, A.; Berndt, J.; Neyts, E. Efficient amorphous platinum catalyst cluster growth on porous carbon: A combined Molecular Dynamics and experimental study. *Appl. Cat. B* **2015**, *62*, 21–26. [CrossRef]
10. Brault, P.; Neyts, E.C. Molecular dynamics simulations of supported metal nanocatalyst formation by plasma sputtering. *Catal. Today* **2015**, *256*, 3–12. [CrossRef]
11. Brault, P.; Chuon, S.; Bauchire, J.-M. Molecular Dynamics simulations of platinum plasma sputtering: A comparative case study. *Front. Phys.* **2016**, *4*, 20. [CrossRef]
12. Brault, P.; Coutanceau, C.; Jennings, P.C.; Vegge, T.; Berndt, J.; Caillard, A.; Baranton, S.; Lankiang, S. Molecular dynamics simulations of ternary $Pt_xPd_yAu_z$ fuel cell nanocatalyst growth. *Int. J. Hydrog. Energy* **2016**, *41*, 22589–22597. [CrossRef]
13. Brault, P. Multiscale Molecular Dynamics Simulation of Plasma Processing: Application to Plasma Sputtering. *Front. Phys.* **2018**, *6*, 59. [CrossRef]
14. Brault, P.; Chamorro-Coral, W.; Chuon, S.; Caillard, A.; Bauchire, J.-M.; Baranton, S.; Coutanceau, C.; Neyts, E.C. Molecular Dynamics simulations of initial Pd and PdO nanocluster growths in a magnetron gas aggregation source. *Front. Chem. Sci. Eng.* **2019**, *13*, 324–329. [CrossRef]
15. Brault, P.; Coutanceau, C.; Caillard, A.; Baranton, S. Pt_3MeAu (Me = Ni, Cu) fuel cell nanocatalyst growth, shapes and efficiency: A molecular dynamics simulation approach. *J. Phys. Chem. C* **2019**, *123*, 29656–29664. [CrossRef]
16. Kouamé, B.S.R.; Baranton, S.; Brault, P.; Canaff, C.; Chamorro-Coral, W.; Caillard, A.; De Oliveira Vigier, K.; Coutanceau, C. Insights on the unique electro-catalytic behavior of PtBi/C materials. *Electrochim. Acta* **2020**, *329*, 135161. [CrossRef]
17. Pikunic, J.; Clinard, C.; Cohaut, N.; Gubbins, K.E.; Guet, J.M.; Pellenq, R.J.M.; Rannou, I.; Rouzaud, J.-N. Structural modeling of porous carbons: Constrained reverse monte carlo method. *Langmuir* **2003**, *19*, 8565. [CrossRef]
18. Brault, P.; Caillard, A.; Baranton, S.; Mougenot, M.; Cuynet, S.; Coutanceau, C. One-step synthesis and chemical characterization of Pt C nanowire composites by plasma sputtering. *ChemSusChem* **2013**, *6*, 1168–1171. [CrossRef]
19. Foiles, S.; Baskes, M.; Daw, M. Embedded-atom-method functions for the fcc metals Cu, Ag, Au, Ni, Pd, Pt, and their alloys. *Phys. Rev. B* **1986**, *33*, 7983. [CrossRef]
20. Tersoff, J. Modeling solid-state chemistry: Interatomic potentials for multicomponent systems. *Phys. Rev. B* **1989**, *39*, 5566. [CrossRef]
21. Graves, D.B.; Brault, P. Molecular dynamics for low temperature plasma–surface interaction studies. *J. Phys. D Appl. Phys.* **2009**, *42*, 194011. [CrossRef]
22. Morrow, B.H.; Striolo, A. Assessing how metal–carbon interactions affect the structure of supported platinum nanoparticles. *Mol. Simul.* **2009**, *35*, 795. [CrossRef]
23. Plimpton, S. Fast Parallel Algorithms for Short-Range Molecular Dynamics. *J. Comp. Phys.* **1995**, *117*, 1–19. [CrossRef]
24. LAMMPS. Molecular Dynamics Simulator. Available online: http://lammps.sandia.gov (accessed on 17 June 2020).
25. Chamorro-Coral, W.; Caillard, A.; Brault, P.; Andreazza, P.; Coutanceau, C.; Baranton, S. The Role of Oxygen on the Growth of Palladium Clusters Synthesized by Gas Aggregation Source. *Plasma Process. Polym.* **2019**, *16*, e1900006. [CrossRef]